Journal of Biomechanics 48 (2015) 162–165

Contents lists available at ScienceDirect

Journal of Biomechanics

journal homepage: www.elsevier.com/locate/jbiomech
www.JBiomech.com

Short communication

High-bandwidth AFM-based rheology is a sensitive indicator of early cartilage aggrecan degradation relevant to mouse models of osteoarthritis

Hadi T. Nia [a], Stephanie J. Gauci [b], Mojtaba Azadi [a], Han-Hwa Hung [c], Eliot Frank [c], Amanda J. Fosang [b], Christine Ortiz [d], Alan J. Grodzinsky [a,c,e,f,*]

[a] Department of Mechanical Engineering, Massachusetts Institute of Technology, Cambridge, MA, United States
[b] University of Melbourne, Department of Paediatrics & Murdoch Children's Research Institute, Royal Childrens Hospital, Parkville, VIC, Australia
[c] Center for Biomedical Engineering, Massachusetts Institute of Technology, Cambridge, MA, United States
[d] Department of Materials Science and Engineering, Massachusetts Institute of Technology, Cambridge, MA, United States
[e] Department of Biological Engineering, Massachusetts Institute of Technology, Cambridge, MA, United States
[f] Department of Electrical Engineering and Computer Science, Massachusetts Institute of Technology, Cambridge, MA, United States

ARTICLE INFO

Article history:
Accepted 8 November 2014

Keywords:
Cartilage
Aggrecan
Nanomechanics
Atomic force microscopy
Osteoarthritis
Mouse model

ABSTRACT

Murine models of osteoarthritis (OA) and post-traumatic OA have been widely used to study the development and progression of these diseases using genetically engineered mouse strains along with surgical or biochemical interventions. However, due to the small size and thickness of murine cartilage, the relationship between mechanical properties, molecular structure and cartilage composition has not been well studied. We adapted a recently developed AFM-based nano-rheology system to probe the dynamic nanomechanical properties of murine cartilage over a wide frequency range of 1 Hz to 10 kHz, and studied the role of glycosaminoglycan (GAG) on the dynamic modulus and poroelastic properties of murine femoral cartilage. We showed that poroelastic properties, highlighting fluid–solid interactions, are more sensitive indicators of loss of mechanical function compared to equilibrium properties in which fluid flow is negligible. These fluid-flow-dependent properties include the hydraulic permeability (an indicator of the resistance of matrix to fluid flow) and the high frequency modulus, obtained at high rates of loading relevant to jumping and impact injury in vivo. Utilizing a fibril-reinforced finite element model, we estimated the poroelastic properties of mouse cartilage over a wide range of loading rates for the first time, and show that the hydraulic permeability increased by a factor ~16 from $k_{normal} = 7.80 \times 10^{-16} \pm 1.3 \times 10^{-16}$ m^4/N s to $k_{GAG\text{-}depleted} = 1.26 \times 10^{-14} \pm 6.73 \times 10^{-15}$ m^4/N s after GAG depletion. The high-frequency modulus, which is related to fluid pressurization and the fibrillar network, decreased significantly after GAG depletion. In contrast, the equilibrium modulus, which is fluid-flow independent, did not show a statistically significant alteration following GAG depletion.

1. Introduction

In recent years, mouse models of osteoarthritis (OA) have received increasing attention due to the ease of creating genetic modifications useful in the search for pathophysiological mechanisms and targets for drug intervention (Fang and Beier, 2014). In addition, recently developed surgical models of joint disease have motivated the use of these genetically engineered mice in models of post-traumatic OA (PTOA) (Fang and Beier, 2014; Little and Hunter, 2013). Large animal studies of OA have typically incorporated correlations between cartilage biomechanical properties and alterations in matrix biochemical composition, since loss of cartilage biomechanical function is a hallmark of joint deterioration. However, measurement of the biomechanical properties of mouse cartilage has been very challenging due to the very small size of the joint and thickness of the cartilage (~50 μm).

During the past 15 years, the first measurements of the mechanical properties of mouse cartilage were reported, initially using micro-indentation (equilibrium stress–strain, Hyttinen, 2001; biphasic creep analysis, Cao et al., 2006) and more recently using high-resolution atomic force microscopy (AFM)-based indentation (Batista et al., 2014; Coles et al., 2010; Darling et al., 2010; Stolz et al., 2009). In the AFM-based studies, however, the

* Corresponding author at: Department of Mechanical Engineering, 500 Technology Sq, Rm 377, Cambridge, MA 02139, United States. Tel.: +1 617 253 4969; fax: +1 617 258 5239.
E-mail address: alg@mit.edu (A.J. Grodzinsky).

http://dx.doi.org/10.1016/j.jbiomech.2014.11.012
0021-9290/

measurements were mostly performed using quasi-static (slow) loading rates in which fluid flow gives little or no contribution to the measured mechanical properties of cartilage. Consistent with this approach, investigators reported the elastic (Young's) modulus of cartilage calculated from such AFM-based indentation measurements. Of course, decades of previous research using much larger tissue specimens (with confined, unconfined and macro-indentation testing configurations) illuminated the importance of intra-tissue fluid flow and pressurization to the poro-viscoelastic properties of cartilage (Ateshian et al., 1997; Lu and Mow, 2008).

We recently adapted AFM-based nanoindentation methodologies to enable measurement of the full-frequency (rate) response of cartilage, including the quasi-static (equilibrium) modulus, the high frequency (instantaneous) elastic response, and the full poroelastic behavior in between these two elastic-like limits (Nia et al., 2011). To further examine the difference between normal and degraded cartilage, we developed a custom-built high-bandwidth AFM-based rheology system (Nia et al., 2013a) to measure the dynamic modulus of cartilage by applying nanoscale deformations (~2 nm) over the wide frequency range of 1 Hz to 10 kHz, a range relevant to joint motions from normal ambulation to the high-frequency content of impact loading (Heiner et al., 2012). (For comparison, a creep measurement, such as that in Cao et al., 2006) would need resolution to the first 10^{-3} s to give data equivalent to that reported here at 1 kHz.) Since measurement in this frequency range is well beyond the capabilities of typical commercial AFMs, this was accomplished by coupling a secondary piezo system within a commercial AFM (Nia et al., 2013b). Using this rheology system with bovine cartilage, we showed that fluid flow-dependent properties, such as hydraulic permeability and the ratio of high frequency modulus to equilibrium modulus are the most sensitive markers of glycosaminoglycan (GAG) depletion, relevant to the early stages of OA (Nia et al., 2013a). The poroelastic material properties of normal and GAG-depleted cartilage were estimated using a fibril-reinforced finite element model (Nia et al., 2011; Soulhat et al., 1999) fit to our dynamic nanoindentation data.

In the present study, we now report for the first time the use this AFM-based high-frequency rheology system to study the nanomechanical poroelastic properties of normal and GAG-depleted murine cartilage. We measured the magnitude and phase angle of the dynamic nanoindentation modulus of murine femoral condyles over a 4-decade frequency range. We show that the dynamic mechanical properties that involve fluid–solid interactions (e.g. hydraulic permeability and the high frequency modulus, the latter not previously reported for murine cartilage) are more sensitive to murine matrix degradation, compared to equilibrium properties (e.g., the equilibrium modulus) where the role of fluid flow is negligible. GAG-depletion (without disrupting the collagen network) caused a significant decrease in high-frequency modulus, where fluid pressurization is critically important (Soltz and Ateshian, 2000), with little change in the equilibrium modulus. We also observed that the hydraulic permeability, representing the resistance of matrix to the fluid flow (Grodzinsky, 2011), increased significantly after GAG-depletion.

2. Materials and methods

2.1. Sample preparation

10–12 Week old C3H mouse knee joints were stored at −20 °C before testing. After thawing, the joints were dissected to expose the femoral condyle, and the femoral bone was glued to stainless disks for AFM-based nano-rheology in a Multimode 4 AFM (Bruker, Billerica, MA) having appropriate optical microscopy to locate indentation sites on the murine condyles. All tested specimens were submerged in PBS with protease inhibitors, as described previously (Batista et al., 2014). The right distal femur of each animal was used as the normal control, and the GAG depletion was performed on the left distal femurs by incubation in 0.1 U/ml chondroitinase-ABC solutions (Sigma) for 48 h, followed by washing several times with PBS.

2.2. AFM specifications and loading profile

AFM colloidal tips 25 μm in diameter and cantilevers with a nominal spring constant $k=40$ N/m were used. (Spring constants were directly measured for all tips using the thermal calibration method (Hutter and Bechhoefer, 1993). We modified the high-frequency nanorheology system, previously designed for use with the MFP3D AFM (Asylum Research) (Nia et al., 2013b) to be coupled to the Bruker Nanoscope 4 AFM (see Fig. S1 in Supplementary material). The applied displacement profile consisted of a ~2 μm pre-indentation (contact radius ~7 μm) and force relaxation to equilibrium; random binary sequence (RBS) displacements with amplitudes of ~2 nm were then applied (Fig. 1c). We used the RBS signal to maximize the signal-to-noise ratio (see Supplementary materials for details). The advantage of the RBS over more traditional signals (e.g., a sinusoidal sweep) is stimulation of the system with relatively higher power, which results in less noisy system identification (i.e., the spectrum of the dynamic modulus (Bozchalooi et al., 2011; Ljung, 1999)). To generate the RBS signal, a sign operator ($\mathrm{sign}(x)=1$ for $x\geq 0$ and $\mathrm{sign}(x)=-1$ for $x<0$) is applied to a set of simulated white Gaussian noise data implemented in LabView (National Instrument Co., Austin, TX). The amplitude of the resulting dataset is then scaled to the maximum allowable excitation given to the secondary piezo actuator. To control the bandwidth of the resulting RBS signal, we applied a low-pass pass filter to the white Gaussian noise prior to the application of the sign operator. In this study, the sampling rate of the measurement was set to $f_s=100$ kHz, the length of the time series was set to $T=20$ s, and the cut-off frequency of the low pass filter was set at $f_c=10$ Hz. Digital-to-analog conversions were performed by data acquisition system NI-USB-6351 (National Instrument Co., Austin, TX).

2.3. Data analysis

A discrete Fourier transform was used to obtain the fundamental frequency component of the force F_{osc} and displacement δ signals (Nia et al., 2013a). The magnitude of the dynamic complex indentation modulus at each frequency was obtained as (Mahaffy et al., 2004):

$$|E^*(f)| = \frac{F_{osc}(f)}{\delta(f)} \frac{1}{2(R\delta_0)^{1/2}} \quad (1)$$

where R is the probe radius and δ_0 is the static offset indentation depth (Fig. 1c). The phase angle ϕ of the dynamic modulus represents the phase of the measured F_{osc} with respect to the applied displacement δ (Fig. 2b). The low-frequency modulus E_L and high-frequency modulus E_H were directly quantified from the

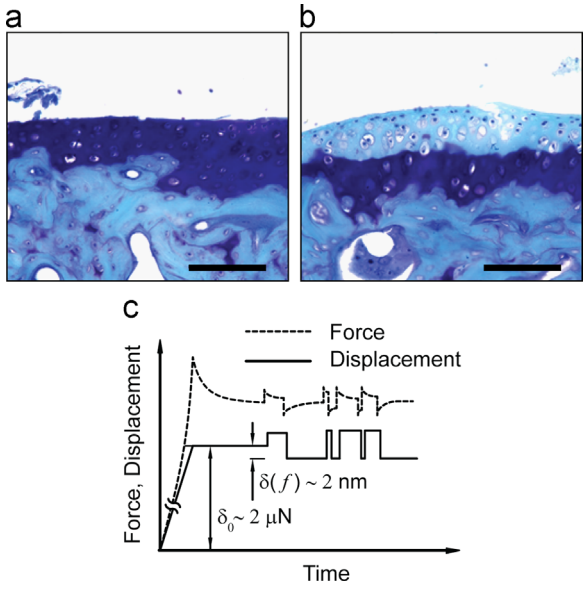

Fig. 1. Histologic image of (a) normal and (b) GAG-depleted femoral condyle cartilage stained with toluidine blue (scale bars, 100 μm). (c) The displacement profile is composed of a ramp-and-hold (displacement of ~2 μm) superimposed by a random binary sequence of steps with amplitude of ~2 nm. (For interpretation of the references to color in this figure legend, the reader is referred to the web version of this article.)

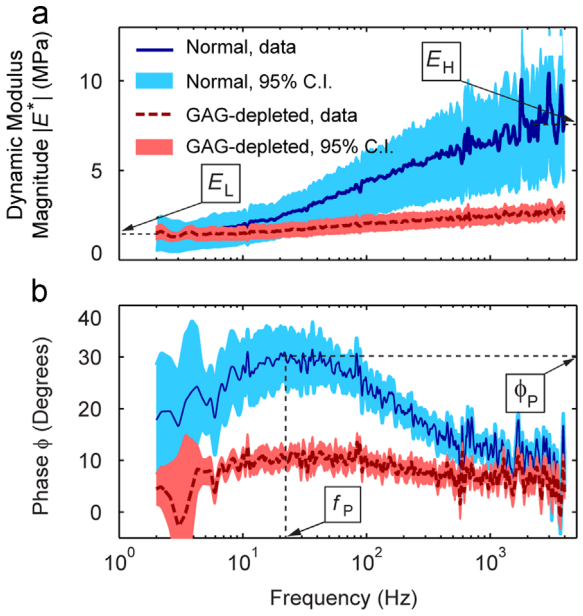

Fig. 2. Wide-frequency (a) magnitude and (b) phase angle of the dynamic modulus of normal (blue) and GAG-depleted (red) cartilage of a typical murine femoral condyle joint shows significant difference in high-frequency modulus E_H, peak phase angle ϕ_P and peak frequency f_P, but not in equilibrium modulus E_L. The solid line is the mean, and the shaded band is the 95% confidence interval based on $M \geq 4$ indentation on different spots on a condyle. (For interpretation of the references to color in this figure legend, the reader is referred to the web version of this article.)

magnitude of the dynamic modulus $|E^*|$ (Fig. 2a). A fibril-reinforced poroelastic model was implemented in which cartilage is approximated as a composite of an isotropic nonfibrillar matrix (representing the proteoglycan constituents), a fibril network (representing collagen fibrils), and a fluid phase (Nia et al., 2011; Soulhat et al., 1999). This model was used to estimate the hydraulic permeability, k, of the nonfibrillar matrix and the Young's modulus of the fibril network, E_f. The drained Poisson's ratio was assumed to be $\nu = 0.1$, the same as that measured in young bovine cartilage (Buschmann et al., 1999). As shown in a previous parametric study (Fig. S1 of Nia et al., 2011), the dynamic mechanical properties were not highly sensitive to Poisson's ratio; the variation in other parameters was less than 10% for $0 < \nu < 0.3$.

2.4. Histology

Fixed (10% formaldehyde) femoral epiphyses were decalcified overnight in Immunocal (United Biosciences), and dehydrated in graded ethanol prior to being processed and embedded in paraffin. Coronal sections (5 μm) were stained with toluidine blue (0.04% toluidine blue in 0.1 M sodium acetate pH 4.0)/fast green (0.1% fast green in deionized water) to identify areas of aggrecan presence and loss.

2.5. Statistics

The data of Fig. 2 are based on $M \geq 4$ indentations on each femoral condyle. The data of Fig. 3 are based on $N = 5$ animals; the mean value for each animal was calculated from $M \geq 4$ indentations on each condyle. The Wilcoxon signed rank test was used to test statistical significance with significance at $p < 0.05$.

3. Results

The histologic images of the normal and GAG-depleted cartilage (Fig. 1a and b) confirmed the loss of aggrecan-GAG following chondroitinase ABC digestion, down to the calcified layer of cartilage (i.e., to a depth of ~30–50 μm as in the typical joint shown in Fig. 1b). The measured low (E_L) and high frequency (E_H) limits of the dynamic modulus magnitude, and the characteristic peak frequency f_{peak} of the dynamic phase angle, were clearly observed for both normal and GAG-depleted cartilage (Fig. 2a and b). Small but non-significant differences in E_L between normal and GAG-depleted cartilage were observed (Figs. 2 and 3a). However,

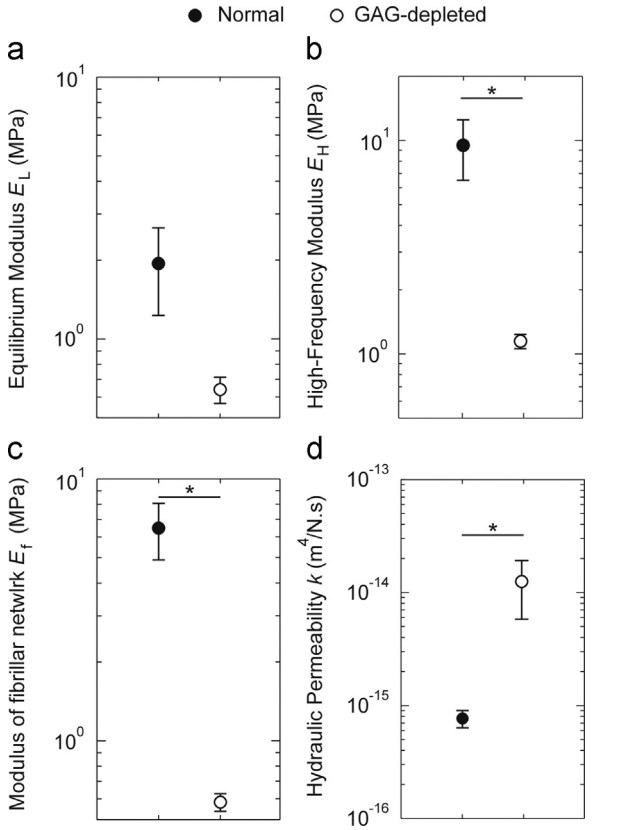

Fig. 3. (a) Equilibrium Modulus E_L, (b) high-frequency modulus E_H, (c) Modulus of fibrillar network E_f and (d) hydraulic permeability k are estimated for normal (black) and GAG-depleted (white) murine femoral condyle cartilage. The data are mean ± SE, $N = 5$ animals. The mean value for each individual animal is based on $M \geq 4$ indentations on each condyle. $^*p < 0.05$, using the nonparametric Wilcoxon signed rank test.

at higher frequencies (equivalent to higher loading rates) the difference between normal and GAG-depleted cartilage was significant (e.g., Figs. 2 and 3b). The calculated hydraulic permeability showed a significant 16-fold increase following GAG depletion (Fig. 3d). The hydraulic permeability for normal cartilage was $k_{normal} = 7.80 \times 10^{-16} \pm 1.3 \times 10^{-16}$ m^4/N s and for GAG-depleted cartilage $k_{GAG\text{-}depleted} = 1.26 \times 10^{-14} \pm 6.73 \times 10^{-15}$ m^4/N s. The equilibrium modulus E_L, however, did not show a statistically significant change despite the decreasing trend in the mean value (Fig. 3a). The modulus of the fibrillar network, E_f, indicative of the contribution of collagen fibers at high loading frequencies when the tissue is pressurized, showed a significant decrease after GAG depletion (Fig. 3c) (The data for each of the 5 animals is shown in Supplementary Fig. S2). The equilibrium modulus E_L measured for normal mouse cartilage is in close agreement with that reported by Cao et al. (2006); slight differences in the reported values of the hydraulic permeability may be due to differences in the tested cartilage location, mouse strain and age, and the details of the indenter (i.e., Cao et al. used a 110 μm diameter plane-ended indenter.

4. Discussion and conclusions

We measured the high-bandwidth dynamic modulus of murine cartilage for the first time over the wide frequency of 1 Hz to 10 kHz, which revealed important dynamic mechanical features such as self-stiffening and energy dissipation in murine cartilage, features that were previously observed only in larger animals having thicker cartilage. The measured frequency-dependent behavior is governed

predominantly by poroelastic mechanisms based on length scale analysis (Nia et al., 2013a, 2011), the quality of the fit between the model (Soulhat et al., 1999) and experimental data, and a comparison between time scales associated with poroelasticity to the longer times (lower frequencies) associated with intrinsic cartilage viscoelasticity (Han et al., 2011). We found that the equilibrium modulus E_L may not be a sensitive indicator of alterations in the extracellular matrix of murine cartilage relevant to the wide range of loading rates that encompass normal ambulation and impact injury. In contrast, we discovered that mechanical properties that involve fluid–solid interactions showed a profound change between normal and GAG-depleted cartilage. One of the key measured fluid-flow-dependent properties is E_H, the dynamic modulus at high loading frequencies (corresponding to running and jumping (Nia et al., 2013a)), where fluid pressurization (Soltz and Ateshian, 2000) occurs even in the ultra-thin cartilage of mice (thickness $\sim$50 μm). The other fluid-flow-dependent property is the hydraulic permeability k, estimated at the nanoscale for both normal and GAG-depleted cartilage utilizing a poroelastic finite element model. The hydraulic permeability increased by an order of magnitude after GAG-depletion, showing the dominant role of aggrecan in defining the pore size within murine cartilage and, hence, resisting the fluid flow that occurs mainly during dynamic loading. After GAG depletion, relevant to the earliest stages of OA, we also observed that the modulus of the fibrillar network, E_f decreased significantly (Fig. 3b). E_f is related to self-stiffening (i.e., the ratio E_H/E_L), an indicator of the pressurization within cartilage, which is caused by dynamic compressive loading. In contrast to bovine cartilage, in which GAG-depletion shifted the dynamic spectrum toward higher frequencies, with E_H and ϕ_{peak} remaining at relatively the same value (Nia et al., 2013a), in murine cartilage, E_H and ϕ_{peak} both decreased significantly after GAG-depletion. Thus, GAG-depleted murine cartilage cannot maintain the pressurization and self-stiffening features of cartilage seen in larger species.

The high-bandwidth AFM-based rheology system appears very useful for (i) evaluating the wide-frequency dynamic mechanical properties of cartilage including impact loading, and (ii) estimating fluid-flow-dependent mechanical properties (e.g., hydraulic permeability and high-frequency (instantaneous) modulus) which are more sensitive to initial matrix degradation than equilibrium properties. Here we reported that this wide-bandwidth measurement can now be measured on murine cartilage, where the use of conventional mechanical tests is limited due to the small size of the murine joint and thickness of the intact articular cartilage layer. We anticipate that studies based on genetically engineered mice and surgical murine models will benefit from the potential of this approach in the search for pathophysiological mechanisms of OA.

Conflict of interest statement

The authors have no conflicts of interest.

Acknowledgements

We thank Dr. Rakesh Jain, Massachusetts General Hospital, for providing the mouse knees. This work was supported by NIH Grant 060331, a Whitaker Health Sciences Fund Fellowship (HTN), and a grant from Arthritis Australia.

Appendix A. Supporting information

Supplementary data associated with this article can be found in the online version at http://dx.doi.org/10.1016/j.jbiomech.2014.11.012.

References

Ateshian, G., Warden, W., Kim, J., Grelsamer, R., Mow, V., 1997. Finite deformation biphasic material properties of bovine articular cartilage from confined compression experiments. J. Biomech. 30, 1157–1164.
Batista, M.A., Nia, H.T., Önnerfjord, P., Cox, K.A., Ortiz, C., Grodzinsky, A.J., Heinegård, D., Han, L., 2014. Nanomechanical phenotype of chondroadherin-null murine articular cartilage. Matrix Biol. 38, 84–90.
Bozchalooi, I., Youcef-Toumi, K., Burns, D., Fantner, G., 2011. Compensator design for improved counterbalancing in high speed atomic force microscopy. Rev. Sci. Instrum. 82, 113712–113712-113712.
Buschmann, M.D., Kim, Y.-J., Wong, M., Frank, E., Hunziker, E.B., Grodzinsky, A.J., 1999. Stimulation of aggrecan synthesis in cartilage explants by cyclic loading is localized to regions of high interstitial fluid flow. Arch. Biochem. Biophys. 366, 1–7.
Cao, L., Youn, I., Guilak, F., Setton, L.A., 2006. Compressive properties of mouse articular cartilage determined in a novel micro-indentation test method and biphasic finite element model. J. Biomech. Eng. 128, 766–771.
Coles, J.M., Zhang, L., Blum, J.J., Warman, M.L., Jay, G.D., Guilak, F., Zauscher, S., 2010. Loss of cartilage structure, stiffness, and frictional properties in mice lacking PRG4. Arthritis Rheum 62, 1666–1674.
Darling, E.M., Wilusz, R.E., Bolognesi, M.P., Zauscher, S., Guilak, F., 2010. Spatial mapping of the biomechanical properties of the pericellular matrix of articular cartilage measured in situ via atomic force microscopy. Biophys. J. 98, 2848–2856.
Fang, H., Beier, F., 2014. Mouse models of osteoarthritis: modelling risk factors and assessing outcomes. Nat. Rev. Rheumatol.
Grodzinsky, A.J., 2011. Fields, Forces, and Flows in Biological Systems. Garland Science, New York, pp. 139–173 (Chapter 4), 259-272, (Chapter 7).
Han, L., Frank, E.H., Greene, J.J., Lee, H.Y., Hung, H.H.K., Grodzinsky, A.J., Ortiz, C., 2011. Time-dependent nanomechanics of cartilage. Biophys. J. 100, 1846–1854.
Heiner, A.D., Martin, J.A., McKinley, T.O., Goetz, J.E., Thedens, D.R., Brown, T.D., 2012. Frequency Content of Cartilage Impact Force Signal Reflects Acute Histologic Structural Damage. Cartilage.
Hutter, J.L., Bechhoefer, J., 1993. Calibration of atomic-force microscope tips. Rev. Sci. Instrum. 64, 1868.
Hyttinen, M., Töyräs, J., Lapveteläinen, T., Lindblom, J., Prockop, D., Li, S., Arita, M., Jurvelin, J., Helminen, H., 2001. Inactivation of one allele of the type II collagen gene alters the collagen network in murine articular cartilage and makes cartilage softer. Ann. Rheum. Dis. 60, 262–268.
Little, C.B., Hunter, D.J., 2013. Post-traumatic osteoarthritis: from mouse models to clinical trials. Nat. Rev. Rheumatol. 9, 485–497.
Ljung, L., 1999. System Identification. Wiley Online Library.
Lu, X., Mow, V., 2008. Biomechanics of articular cartilage and determination of material properties. Med. Sci. Sports Exercise 40, 193.
Mahaffy, R.E., Park, S., Gerde, E., Kas, J., Shih, C.K., 2004. Quantitative analysis of the viscoelastic properties of thin regions of fibroblasts using atomic force microscopy. Biophys. J. 86, 1777–1793.
Nia, H.T., Bozchalooi, I.S., Li, Y., Han, L., Hung, H.-H., Frank, E., Youcef-Toumi, K., Ortiz, C., Grodzinsky, A., 2013a. High-bandwidth AFM-based rheology reveals that cartilage is most sensitive to high loading rates at early stages of impairment. Biophys. J. 104, 1529–1537.
Nia, H.T., Bozchalooi, I.S., Youcef-Toumi, K., Ortiz, C., Grodzinsky, A.J., Frank, E., 2013b. High-frequency Rheology System. US Patent 8,516,610.
Nia, H.T., Han, L., Li, Y., Ortiz, C., Grodzinsky, A., 2011. Poroelasticity of cartilage at the nanoscale. Biophys. J. 101, 2304–2313.
Soltz, M.A., Ateshian, G.A., 2000. Interstitial fluid pressurization during confined compression cyclical loading of articular cartilage. Ann. Biomed. Eng. 28, 150–159.
Soulhat, J., Buschmann, M.D., Shirazi-Adl, A., 1999. A fibril-network-reinforced biphasic model of cartilage in unconfined compression. J. Biomech. Eng. 121, 340.
Stolz, M., Gottardi, R., Raiteri, R., Miot, S., Martin, I., Imer, R., Staufer, U., Raducanu, A., Duggelin, M., Baschong, W., Daniels, A.U., Friederich, N.F., Aszodi, A., Aebi, U., 2009. Early detection of aging cartilage and osteoarthritis in mice and patient samples using atomic force microscopy. Nat. Nanotechnol. 4, 186–192.